



Delft University of Technology

Combined effect of hysteresis and heterogeneity on the stability of an embankment under transient seepage

Liu, Kang; Vardon, Phil; Hicks, Michael; Arnold, Patrick

DOI

[10.1016/j.enggeo.2016.11.011](https://doi.org/10.1016/j.enggeo.2016.11.011)

Publication date

2017

Document Version

Accepted author manuscript

Published in

Engineering Geology

Citation (APA)

Liu, K., Vardon, P., Hicks, M., & Arnold, P. (2017). Combined effect of hysteresis and heterogeneity on the stability of an embankment under transient seepage. *Engineering Geology*, 219, 140-150.
<https://doi.org/10.1016/j.enggeo.2016.11.011>

Important note

To cite this publication, please use the final published version (if applicable).

Please check the document version above.

Copyright

Other than for strictly personal use, it is not permitted to download, forward or distribute the text or part of it, without the consent of the author(s) and/or copyright holder(s), unless the work is under an open content license such as Creative Commons.

Takedown policy

Please contact us and provide details if you believe this document breaches copyrights.

We will remove access to the work immediately and investigate your claim.

Combined effect of hysteresis and heterogeneity on the stability of an embankment under transient seepage

Liu, K., Vardon, P.J., Hicks, M.A., Arnold, P.

Geo-Engineering Section, Faculty of Civil Engineering and Geosciences, Delft

University of Technology, The Netherlands

7 **Abstract:** The stability of most earth embankments is strongly influenced by the
8 water content of the soil. The water content directly influences the suction or pore
9 pressure in the soil, as well as the mass of material, thereby affecting the stress state
10 and strength, and leading to changes in the stability. These aspects are coupled by
11 the so-called soil water retention behaviour, which is observed to be a hysteretic
12 phenomenon. Moreover, soils are known to be spatially variable or heterogeneous in
13 nature, which can lead to preferential flow paths and stronger or weaker zones. In
14 this paper the behaviour of a heterogeneous earth embankment subjected to cyclic
15 water level fluctuation, including the impact of hysteresis, is investigated. The soil
16 property values governing the unsaturated hydraulic response of the embankment
17 are considered as spatially random variables, with the mechanical property values
18 considered deterministic in order to isolate the impact of the hydraulic behaviour.
19 The Monte Carlo Method (MCM) is used to conduct probabilistic analyses and an
20 assessment of the relative influence of material properties illustrates that the
21 saturated hydraulic conductivity, k_{sat} , plays a dominant role in the slope stability.
22 Moreover, in the initially drying condition, the average factor of safety (FOS) and the

23 95th percentile FOS of the slope considering hysteresis are smaller than those
24 without considering hysteresis, at all times, while the variability of the FOS
25 considering hysteresis is larger than that when not considering hysteresis. In practice,
26 this means that slopes under seepage conditions, which are assessed to have a low
27 FOS, should be assessed including the hysteretic behaviour to ensure stability.

28 **Keywords:** Embankment, hysteresis, reliability, slope stability, spatial variability,
29 transient seepage

30 **1. Introduction**

31 Slopes under seepage conditions, with both saturated and unsaturated zones, are
32 common and of great concern in geotechnical engineering (Chen and Zhang, 2006;
33 Rahardjo et al., 2010). The saturated–unsaturated seepage in the slope has a
34 significant impact on the slope stability, via changes in shear strength and volumetric
35 weights, and is strongly related to the water retention behaviour of the unsaturated
36 soil (Gui et al., 2000; Le et al., 2012; Zhu et al., 2013; Zhang et al., 2015; Zhang et al.,
37 2016).

38 The soil water retention curve (SWRC) describes the relationship between the
39 suction head, h_s , and a measure of the water content, in this paper the volumetric
40 water content (VWC), θ , and in addition impacts the hydraulic conductivity, k ,
41 which further affects the distribution of pore water pressure (PWP) in the soil (Lam
42 et al., 1987; Yang et al., 2012). Hysteresis in the water retention behaviour of
43 unsaturated soils describes a non-unique relationship between h_s and θ , and thus

44 also between h_s and k (Jaynes, 1984; Pham et al., 2005; Wu et al., 2012).
45 Moreover, due to the existence of hysteresis, the VWC in the soil under cyclic drying
46 and wetting processes may exhibit a significantly different response as compared to
47 the non-hysteretic case (Ma et al., 2011). Indeed, the differences in the PWP and
48 VWC induced by the hysteresis in the SWRC contribute to a hysteretic shear strength
49 response which affects the stability and reliability of the slope (Bishop, 1959).

50 However, to simplify seepage analyses the effect of hysteresis is commonly
51 ignored (e.g. Tsaparas et al., 2002; Le et al., 2012), even though it may generate
52 inaccurate predictions of the distributions of PWP and VWC. Tami et al. (2004)
53 investigated the variation in the suction profile in a soil column with a hysteretic
54 SWRC. It was found that, due to the hysteresis, the suction at the newly reached
55 steady state after a certain period of infiltration was significantly affected by the
56 initial water content prior to the infiltration process. Yang et al. (2012) studied the
57 variation of matric suction and VWC in a soil column under cyclic precipitation and
58 evaporation. It was found that the computed results were closer to the experimental
59 results when considering hysteresis.

60 Recently, several researchers have investigated the effect of hysteresis on the
61 stability of soil slopes. Ebel et al. (2010) pointed out that simulations ignoring
62 hysteresis could underestimate the potential for landslides. Ma et al. (2011)
63 conducted an experimental and numerical study of a soil slope to assess the effect of
64 hysteresis, both on the hydraulic response and the slope stability. It was found that
65 the distribution of water content was influenced by hysteresis and that the calculated

66 FOS of the slope considering hysteresis recovered quickly after rainfall and was larger
67 than that without considering hysteresis for any given time.

68 Most research that includes the effect of hysteresis focuses on homogeneous
69 soils. Conversely, if the heterogeneity of soil property values is taken into account,
70 the impact of hysteresis is typically not accounted for (Arnold and Hicks, 2010; 2011;
71 Zhu et al., 2013). However, Nakagawa et al. (2012) highlighted the importance of
72 considering both hysteresis and heterogeneity in the simulation of unsaturated flow
73 by comparing numerical results with experimental data. Very few studies have
74 incorporated hysteresis and heterogeneity in the assessment of slope stability. Yang
75 et al. (2013) accounted for the effect of hysteresis and spatial variability of soil
76 property values, i.e. of the saturated hydraulic conductivity and some SWRC fitting
77 parameters, in a one-dimensional infiltration problem. It was shown that the
78 combined effect of hysteresis and heterogeneity of soil property values increased the
79 uncertainty in the estimation of the ability to prevent penetration in soil covers,
80 compared to the non-hysteretic but heterogeneous case. Zhang (2007) incorporated
81 both hysteresis and heterogeneity into the stability analysis of a 2D slope under cyclic
82 precipitation and evaporation, with the analysis starting on the wetting SWRC. The
83 results suggested that simulations without considering the effect of hysteresis may
84 underestimate the slope reliability.

85 This paper investigates the slope stability of an embankment under transient
86 seepage, i.e. due to a cyclic external water level. The effects of both hysteresis and
87 heterogeneity of the soil property values on the seepage response are considered.

88 First, the mechanical and stochastic model framework for slope stability under
89 saturated–unsaturated seepage is briefly introduced. Next, the numerical
90 implementation of the framework is explained, and a specific example then utilised
91 to investigate the impact of considering hysteresis for a homogeneous embankment.
92 Finally, the effect of spatial variability of the soil property values is considered, by
93 conducting a probabilistic analysis of the slope stability and comparing the results of
94 the hysteretic and non-hysteretic cases.

95 **2. Formulation**

96 **2.1 Governing flow equation**

97 The governing equation of 2D transient unsaturated–saturated flow is based on mass
98 conservation. In the flow analysis, the soil skeleton is considered to be rigid, which
99 means that any volume change during the seepage process is not accounted for.
100 Therefore, the governing flow equation, in incremental form, is (e.g. Celia et al.,
101 1990)

$$102 \quad \frac{\partial}{\partial x} \left(k_x \frac{\partial h}{\partial x} \right) + \frac{\partial}{\partial z} \left(k_z \frac{\partial h}{\partial z} + k_z \right) = C(h) \frac{\partial h}{\partial t} \quad (1)$$

103 where k_x and k_z are the hydraulic conductivities in the x and z directions,
104 respectively, h is the PWP head, t is time and $C(h) = \partial\theta/\partial h$ is the specific
105 moisture capacity function with θ being the VWC. The same description of mass
106 conservation can be used for heterogeneous porous media (e.g. Gui et al., 2000) with
107 an appropriate selection of hydraulic conductivities at each location.

108 **2.2 Water retention behaviour**

109 The SWRC is a function relating the suction head, h_s , with θ . The suction head is

110 defined as the negative component of h and is represented by

$$111 \quad h_s = -h = s/\gamma_w = (u_a - u_w)/\gamma_w \quad (2)$$

112 where s is the matric suction, u_a is the pore air pressure, which is assumed to be

113 atmospheric in this paper, u_w is the PWP and γ_w is the unit weight of water.

114 The van Genuchten (1980) model is frequently used to describe the SWRC (e.g.

115 Gui et al., 2000; Sivakumar Babu and Murthy, 2005; Phoon et al., 2010) as it can give

116 a good approximation of the experimental results of many soil types (e.g. Han et al.,

117 2010). It is given by

$$118 \quad S = \frac{\theta - \theta_r}{\theta_s - \theta_r} = \begin{cases} \frac{1}{[1 + (\alpha|h|^n)]^m} & h < 0 \\ S = 1 & h \geq 0 \end{cases} \quad (3)$$

119 where S is effective degree of saturation, α is a parameter which is approximately

120 the inverse of the air-entry suction head, $h_{s,ae}$, and θ_s and θ_r are the saturated

121 and residual VWC, respectively (see Figure 1 (a)). Due to the hysteretic behaviour

122 described by the water retention curve, the main wetting and drying curves have

123 different values of α , i.e. $\alpha_w \approx \frac{1}{h_{s,ae,w}} > \alpha_d \approx \frac{1}{h_{s,ae,d}}$. The model parameter n

124 defines the slope of the water retention curve, which is here assumed to be identical

125 for the main wetting and drying responses, and m is a curve fitting parameter which

126 is here approximated (Mualem, 1976) by

$$127 \quad m = 1 - 1/n \quad (4)$$

128 The hydraulic conductivity of the unsaturated soil is typically a function of the

129 effective degree of saturation (Figure 1 (b)). It can be derived from the SWRC by

130 using the van Genuchten (1980) model, for which one common expression is

131

$$k = k_{sat} \sqrt{S} [1 - (1 - S^{(n/n-1)})^m]^2 \quad (5)$$

132 where k_{sat} is the saturated hydraulic conductivity of the soil. It can be seen from
133 Figure 1 that, due to the hysteresis in the SWRC, there will be also hysteresis in the
134 hydraulic conductivity function with respect to the suction head.

135 Jaynes (1984) compared four methods of modelling hysteresis in the water
136 retention behaviour, i.e. in approximating the curves between the main wetting and
137 drying curves, referred to as scanning curves, (see Figure 1 (a)), and found that the
138 performance of the four methods were equally good in the numerical simulation of
139 hysteretic flow. Furthermore, the author pointed out that, due to simplicity, linear
140 scanning curves were often used in numerical analyses. Therefore, as this paper is
141 not considering a specific soil, this approach has been adopted here to describe the
142 transition from wetting to drying and vice versa (Figure 1 (a)), utilising parameter κ
143 to define the gradient of the curves.

144 **2.3 Slope stability assessment**

145 Slope stability equilibrium is solved using a linear elastic, perfectly plastic material
146 model. Bishop's effective stress combined with the extended Mohr–Coulomb failure
147 criterion has been used to model the shear strength (Bishop, 1959):

148

$$\tau = c' + \sigma_t \tan\varphi' + \chi s \tan\varphi' \quad (6)$$

149 where τ is the shear strength, c' and φ' are the effective cohesion and friction
150 angle, χ is a scalar parameter defining the suction-induced effective stress, s is the
151 matric suction and σ_t is the total stress normal to the sliding plane (Cai and Ugai,
152 2004). In this paper, the suction stress, χs , is defined as

$$\begin{aligned} 153 \quad \chi s &= S_s = \frac{\theta - \theta_r}{\theta_s - \theta_r} s & s > 0 \\ &\chi s = S_s = s & s \leq 0 \end{aligned} \quad (7)$$

154 where the suction stress is assumed to equal the effective degree of saturation
155 (Vanapalli et al., 1996). When the suction is negative, i.e. there is a positive PWP, the
156 conventional effective stress is used.

157 The unit weight, γ , of the unsaturated soil is a function of θ (Tsai and Chen,
158 2010) and can be expressed as

$$159 \quad \gamma = [(1 - \theta_s)\rho_w G_s + \rho_w \theta]g \quad (8)$$

160 where ρ_w is the density of water, G_s is the specific gravity of the soil particles and
161 g is the gravitational acceleration.

162 **2.4 Spatial variability of soil properties**

163 The heterogeneity of the soil is considered by some soil property values being
164 spatially random variables following normal or lognormal distributions. The point
165 statistics of the variables are described by the distribution type, mean, variance and
166 cross-correlation between different variables. The coefficient of variation (COV) is a
167 normalised measure of the variability, defined as

$$168 \quad COV = \frac{\sigma}{\mu} \quad (9)$$

169 where μ and σ are the mean and standard deviation, respectively.

170 The soil property values are also spatially correlated due to the deposition
171 process. The scale of fluctuation, l , is the distance over which parameter values are
172 significantly correlated (Fenton and Vanmarcke, 1990). In addition, the deposition
173 process causes different scales of fluctuation in the horizontal and vertical directions.
174 Hence, the ratio of the horizontal scale of fluctuation to the vertical scale of

175 fluctuation is referred to as the degree of anisotropy of the heterogeneity, ξ (Hicks
176 and Samy, 2002; 2004), i.e.

177
$$\xi = \frac{l_h}{l_v} \quad (10)$$

178 where l_h and l_v are the horizontal and vertical scales of fluctuation, respectively.

179 For more information about the statistics of soil property values, the reader may
180 refer to Phoon and Kulhawy (1999).

181 **3 Numerical implementation**

182 **3.1 Slope stability under transient seepage**

183 The flow and slope stability analyses both use finite element (FE) programs that have
184 been developed based on Smith et al. (2013); that is, using 4-node quadrilateral
185 elements for the flow analysis and 8-node quadrilateral elements for the slope
186 stability analysis. First, a flow analysis is performed and the variation of suction stress
187 and VWC with time, i.e. $\chi s(t)$ and $\theta(t)$, are computed. Next, the suction stress and
188 VWC from the flow analysis are imported into the slope stability FE program and
189 mapped onto the Gauss points for computing the effective stresses due to
190 gravitational (self-weight) loading.

191 The governing flow equation has been solved by using the modified Picard
192 iteration method (Celia et al., 1990; Lehmann and Ackerer, 1998). In the flow analysis
193 program, the VWC for the main drying and wetting curves is computed via Equation 3.
194 The water retention behaviour along the linear scanning curve is computed via an
195 algorithm proposed by Yang et al. (2011), in which the VWC at the current time,
196 $t + 1$, is determined as a function of the current change in suction head and the

197 previous VWC, i.e. $\theta^{t+1} = f(\Delta h_s^{t+1}, \theta^t)$.

198 If the PWP at the Gauss point is negative, the soil unit weight is updated by
199 Equation 8 in the FE slope stability analysis; otherwise the unit weight is equal to the
200 saturated unit weight. The strength reduction method (Griffiths and Lane, 1999) has
201 then been applied to compute the FOS of the slope. In this method, the FOS is
202 defined as the factor by which the original shear strength is reduced in order to
203 cause the slope to fail. Hence,

204

$$\begin{aligned} c'_f &= c' / \text{FOS} \\ \varphi'_f &= \arctan\left(\frac{\tan \varphi'}{\text{FOS}}\right) \end{aligned} \quad (11)$$

205 where c'_f and φ'_f are the factored shear strength parameters at slope failure.

206 3.2 Probabilistic simulation

207 For modelling soil heterogeneity, the Local Average Subdivision (LAS) method (Fenton
208 and Vanmarcke, 1990) has been used to generate stationary, spatially correlated,
209 random fields of soil parameter values. In this paper, the exponential Markov
210 correlation function has been used to model the correlation between the parameter
211 values at different locations:

$$212 \rho(\tau) = \exp\left(-\frac{2}{l}\tau\right) \quad (12)$$

213 where τ is the lag distance between two points at different locations in space within
214 the random field, and l is the scale of fluctuation.

215 The Monte Carlo Method (MCM) has been used to investigate the
216 characteristics of the slope stability under stochastic transient seepage. Each Monte
217 Carlo simulation involves multiple realisations of the problem, in which each random

218 field is based on the same set of statistics, but yields a unique representation of the
219 spatial variation in a material property. Individual random fields are generated for
220 each soil parameter in standard normal space, and then transformed into physical
221 space. The random field cell values of the parameters, generated by LAS, are mapped
222 onto the finite element mesh at the Gauss point level.

223 In this investigation, for the purpose of comparing non-hysteretic and hysteretic
224 responses, 1000 realisations was found to be sufficient, as well as being consistent
225 with other studies, e.g. Griffiths and Fenton (2004), Hicks and Spencer (2010) and
226 Santoso et al. (2011).

227 **4. Slope stability example**

228 A heterogeneous embankment subjected to cyclic external water level fluctuation
229 has been taken as an example to demonstrate the influence of the combined effect
230 of hysteresis and heterogeneity on slope stability. For comparative purposes, the
231 investigation has also included non-hysteretic and homogeneous analyses.

232 The geometry of the embankment is shown in Figure 2. Its height is 12 m, and
233 the width of its crest and base are 4 m and 52 m, respectively. The embankment
234 experiences a water level fluctuation on its upstream side. WL1 and WL2 are the
235 highest and lowest water levels, whereas line A-A (at $x = 34$ m) and point B (at
236 $x = 28$ m) denote the observation cross-section and point where results are
237 recorded. The downstream water level remains at foundation level ($z = 0$ m), and
238 the bottom boundary of the embankment is impermeable and fixed.

239 The water level fluctuation with time has been simulated by the summation of

240 two sinusoidal curves, with two different frequencies (denoted by functions C_1 and
241 C_2 in Figure 3). For both curves, the mean and amplitude are 3.5 m and 3 m
242 respectively, whereas the time period of C_1 , termed T_1 (and equal to 10 days), is
243 three times that of C_2 . The resulting water level fluctuation, shown by the green line
244 in Figure 3, has a maximum water level of 10 m (WL1) and a minimum water level of
245 4 m (WL2).

246 The parameter values of the deterministic homogenous case, in which the
247 spatial variability of parameters is not included, are listed in Table 1, with the SWRC
248 properties following Yang et al. (2011) and the mechanical properties following Hicks
249 and Spencer (2010). The specific gravity is typical of an organic soil, i.e. ~2, as is the
250 hydraulic conductivity, at 1×10^{-6} m/s. The SWRC is given in Figure 4. In the
251 non-hysteretic case, the drying property values are used (as explained in Section 5.1).
252 For the heterogeneous case, in which several hydraulic parameters are spatially
253 random, the distributions of these parameters are listed in Table 2. Nielsen et al.
254 (1973), Freeze (1975) and ASCE (2008) have shown that k_{sat} can be assumed to be
255 log-normally distributed, and a $COV_{k_{sat}}$ of 0.9 to 1.0 was reported in Nielsen et al.
256 (1973). α_d has also been described as log-normally distributed (Carsel and Parris,
257 1988; Russo and Bouton, 1992; de Rooij et al., 2004) and, in Carsel and Parris (1988),
258 COV_{α_d} is from 0.203 to 1.603. Russo and Bouton (1992) suggested a normal
259 distribution for n , while Carsel and Parris (1988) indicated that COV_n is from 0.033
260 to 0.203. De Rooij et al. (2004) showed that the distribution of θ_s is log-normal,
261 while Carsel and Parris (1988) reported that COV_{θ_s} is from 0.15 to 0.355. In de Rooij

262 et al. (2004), COV_{θ_r} is equal to 0.031 and the distribution is assumed to be
263 log-normal.

264 **5 Results**

265 In the following numerical investigation, the effects of hysteresis, parameter variation
266 and heterogeneity are systematically investigated. In Section 5.1, hysteresis in
267 isolation, i.e. a homogenous embankment, has been studied, in Section 5.2 the
268 influence of the variable parameters is investigated and in Section 5.3 the impact of
269 hysteresis on a spatially variable embankment has been presented. Table 3,
270 summarises the items investigated in each sub-section.

271 **5.1 Influence of hysteresis on the seepage and stability of a homogeneous
272 embankment**

273 Several analyses were initially undertaken to find an optimal mesh size and time step
274 which would ensure both accuracy and efficiency. A standard finite element size of
275 0.5 m (vertical) by 1.0 m (horizontal) was selected and the time step was chosen to
276 be 0.05 d.

277 In Liu et al. (2015), the current authors illustrated that hysteretic water retention
278 behaviour significantly influenced the water flow and soil suction distributions in the
279 embankment, and thereby the slope stability. Figure 5 shows the variation of the FOS
280 with time. It increases from the initial conditions, illustrating the benefit of
281 undertaking transient analysis. For both the hysteretic and non-hysteretic cases, the
282 FOS is seen to react to the change in water level, where, if the water level is high, the
283 FOS is low and vice versa. Figure 5 shows that, at any instant in time, the FOS of the

284 hysteretic case is always smaller than that of the non-hysteretic case, due to the
285 selection of the main drying curve as the starting point of the transient seepage
286 analysis for both cases. The reason for choosing the main drying curve is that Ebel
287 (2010) reported it to be the most easily measured in the laboratory and therefore the
288 most frequently used. In addition, in the numerical example, the embankment first
289 experiences water level drawdown, i.e. a drying process. If the non-hysteretic SWRC
290 is instead taken to be the wetting curve, a difference in the FOS between the
291 non-hysteretic and hysteretic cases would still exist, although the FOS of the
292 hysteretic case would then be bigger than that of the non-hysteretic case.

293 In Figure 5, the hysteretic case reacts quicker to changes in water level due to
294 the variation of VWC with suction moving along the scanning curve, and this, in
295 general, leads to a more significant and faster reduction in the FOS when the water
296 level rises. The largest difference coincides with the highest water level and lowest
297 FOS (ignoring the first part which is affected by the initial conditions). It is
298 emphasised that in this analysis, all properties are constant throughout the domain,
299 and no heterogeneity is considered. Section 5.3 provides a demonstration of the
300 impact of considering heterogeneity alongside hysteresis.

301 Figure 6 compares the PWP head and VWC variation with time between the
302 non-hysteretic and hysteretic cases, at three depths along cross-section A-A (see
303 Figure 2). It can be seen that the VWC of the hysteretic case is usually larger or equal
304 to that of the non-hysteretic case, and that the PWP head of the hysteretic case is
305 also usually larger or equal to the non-hysteretic case. The larger the VWC, the larger

306 the overturning moment due to the greater soil weight; in addition, the smaller
307 suction head results in a smaller shear resistance to sliding. Therefore, the combined
308 effects lead to the FOS in the hysteretic case being smaller than in the non-hysteretic
309 case (Figure 5).

310 In Figure 6, it is seen that the PWP head in the hysteretic case can change more
311 rapidly than that in the non-hysteretic case, due to the suction head moving along
312 the scanning curves. In addition, it can be seen that the pore pressures are more
313 sensitive to boundary condition (i.e. external water level) changes in the hysteretic
314 case, with a similar change for different depths as seen from the blue curves in the
315 left plots of Figure 6. In the non-hysteretic case, the red curve describing the highest
316 point (Figure 6 (a)) does not change significantly with a change of boundary
317 condition, whereas that describing the lowest point is almost as sensitive as in the
318 hysteretic case. The response delay of the non-hysteretic case during transient
319 seepage can be explained by referring to the wetting and drying process in a soil
320 column (Yang et al., 2011; 2012).

321 The state at any point in the slope domain may be categorised into three types:
322 always unsaturated, saturated–unsaturated and always saturated. The suction
323 variations at typical points representing these three cases are illustrated in Figure 7,
324 which shows the variation of the VWC with suction for points 1–3 shown in Figure 2.
325 Figures 7(a) and (b) denote point 1 which is always in the unsaturated condition;
326 Figures 7(c) and (d) denote point 2 which changes between saturated and
327 unsaturated conditions; and Figures 7(e) and (f) denote point 3 which is always in the

328 saturated condition. In Figure 7, it can be noted that the suction in the hysteretic
329 case shows larger variation than that in the non-hysteretic case, due to the suction
330 head varying in the area enclosed by the main drying and wetting curves.

331 **5.2 Relative importance of hydraulic parameters**

332 To investigate the hydraulic parameters that are here represented by statistical
333 distributions, i.e. $\mathbf{X} = [k_{sat}, \alpha_d, n, \theta_s, \theta_r]$, a sensitivity analysis has been undertaken
334 to assess their relative importance on the embankment response under both
335 non-hysteretic and hysteretic conditions. Gardner et al. (1981) suggested the use of
336 the correlation coefficient derived from Monte Carlo simulation to evaluate the
337 relative importance of the input parameters on the output. Hence, one thousand
338 values from the distribution of each parameter (Table 2) have been randomly
339 sampled, and assembled into a 1000×5 input matrix:

$$340 \begin{bmatrix} \mathbf{X}_1 \\ \vdots \\ \mathbf{X}_{1000} \end{bmatrix} = \begin{bmatrix} k_{sat,1} & \alpha_{d,1} & n_1 & \theta_{s,1} & \theta_{r,1} \\ \vdots & & \ddots & & \vdots \\ k_{sat,1000} & \alpha_{d,1000} & n_{1000} & \theta_{s,1000} & \theta_{r,1000} \end{bmatrix} \quad (12)$$

341 No correlation is assumed between the parameters, although physically likely due to
342 the dependence on grain size, mineralogy and density, as the purpose of this
343 investigation is to assess which of the parameters is important in controlling the
344 system response.

345 Each combination of the random values of the five parameters (one row in the
346 matrix) were utilised in a transient seepage analysis (with the domain being taken as
347 homogeneous). The Pearson correlation coefficient was then utilised to give a
348 measure of the correlation between two variables, and is defined as

349

$$\rho_{x_i, \text{FOS}} = \frac{\text{COV}(x_i, \text{FOS})}{\sigma_{x_i} \sigma_{\text{FOS}}} = \frac{E[(x_i - \mu_{x_i})(\text{FOS} - \mu_{\text{FOS}})]}{\sigma_{x_i} \sigma_{\text{FOS}}} \quad (13)$$

350 where x_i is the i th random variable in \mathbf{X} , $\rho_{x_i, \text{FOS}}$ is the Pearson correlation
 351 coefficient, $\text{COV}(x_i, \text{FOS})$ is the covariance of the two variables, and σ_{x_i} and σ_{FOS}
 352 are the standard deviation of x_i and FOS, respectively.

353 Figure 8 shows the Pearson correlation coefficients between the FOS and
 354 different hydraulic parameters for the non-hysteretic case at time $t = 2T_2$. The black
 355 values are for the entire data set and the red values are for FOS below 1.25. It can be
 356 seen that the FOS increases with an increase in k_{sat} , but decreases with increasing
 357 α_d , n and θ_s . The positive relationship between k_{sat} and FOS is because, when
 358 k_{sat} is large, the outflow of water is faster, leading to a higher FOS. The negative
 359 correlations between FOS and α_d , n and θ_s may be explained with the aid of
 360 Figure 9, which illustrates the sensitivity of the SWRC equation to the different
 361 parameters, and by recalling that a lower FOS is generally obtained for higher VWC
 362 and lower suction. With reference to Figure 9, for curves ① and ②, the only
 363 difference is in the value of parameter θ_s , where $\theta_{s1} > \theta_{s2}$. An increase in θ_s
 364 means that the detained water in the embankment increases, which induces a lower
 365 FOS. For curves ② and ④, the only difference is parameter α_d , where $\alpha_{d2} < \alpha_{d4}$.
 366 For the same VWC, the suction is larger for α_{d2} and this causes a higher FOS. For
 367 curves ② and ③, the only difference is parameter n , where $n_2 < n_3$. For the
 368 same VWC, the suction is larger for n_2 and this causes a higher FOS. Figure 8 shows
 369 that θ_r has almost no influence on the FOS, because the suction cannot reach the
 370 range of values where the value of θ_r has a large influence. The values of the

371 Pearson correlation coefficients for FOS<1.25 were calculated to investigate whether
372 FOS closer to failure had similar correlations to those of the whole dataset. All trends
373 are similar, in that positive correlations remain positive and vice versa, although the
374 correlations are lower due to the removal of higher calculated FOS. However, there is
375 still a strong positive correlation between FOS and k_{sat} .

376 Figure 10 shows the correlation coefficients as a function of time. The left
377 vertical axis applies to the solid lines and the right axis applies to the dashed lines. In
378 Figure 10, the correlation coefficients significantly decrease for three hydraulic
379 parameters, i.e. for k_{sat} , α_d and n , whereas the correlation coefficients for θ_s
380 and θ_r remain fairly stable. This is due to the impact of the propagation of water in
381 the embankment, induced by the upstream water level fluctuation, towards the
382 downstream. At the end of the first main cycle ($T_1 = 10$ d) the water level has
383 returned to its highest position, so that the unsaturated zone in the sliding area has
384 become smaller. In addition, the water flowing into the embankment due to the
385 increasing external water level has not had time to drain out from the downstream
386 side. These factors result in the FOS reducing, even when k_{sat} is relatively high and
387 α_d and n are relatively small. Hence, when the data of the three parameters versus
388 FOS, for $t = T_1 = 3T_2$, are plotted in the same way as in the first three plots in
389 Figure 8 (though not shown here), the dots become more scattered and the
390 correlation coefficients decrease.

391 As was seen in Figure 8, Figure 10 shows that the saturated hydraulic
392 conductivity has the largest influence on the FOS, while the residual VWC has almost

393 no influence. Indeed, the correlation coefficient between the FOS and k_{sat} remains
394 high in comparison with the other parameters, even at its lowest point, which
395 indicates that k_{sat} plays a dominant role in the final computation of the FOS.
396 Therefore, only the heterogeneity of k_{sat} has been incorporated into the transient
397 seepage analysis in the following section. This conclusion is also supported by other
398 studies reported in literature. Rahardjo et al. (2007) pointed out that the saturated
399 hydraulic conductivity played a dominant role in rainfall infiltration compared to
400 other hydraulic parameters. Avanidou and Paleologos (2002) and Chen et al. (1994a,
401 1994b) also suggested that the saturated hydraulic conductivity was the most
402 important parameter in unsaturated heterogeneous soils. Zhang et al. (2005) studied
403 rainfall-induced slope failure in a heterogeneous slope. In the study, only the
404 saturated hydraulic conductivity, saturated volumetric water content, the parameter
405 related to the air entry value and the slope of the water retention curve were
406 considered to be variable, because these four parameters were considered to be
407 important and influence the computation of slope stability. The residual volumetric
408 water content was considered to be not important.

409 **5.3 Influence of hysteresis on the seepage and stability of a heterogeneous**
410 **embankment**

411 In this section, a spatially variable saturated hydraulic conductivity is used and both
412 hysteretic and non-hysteretic SWRCs are considered; all other parameters are
413 constant. As an indicative example, the scale of fluctuation, $l_{lnk_{sat}}$, has been taken
414 to be 1.0 m in both the vertical and horizontal directions, i.e. giving isotropic

415 variability, and 1000 realisations have been performed. Note that, for more
416 comprehensive conclusions on the influence of spatial variability, further studies are
417 needed.

418 **5.3.1 Influence of hysteresis on stochastic seepage**

419 In Figure 11, the VWCs at Point B from Figure 2 at $t = T_1 = 10$ d are compared (one
420 dot from each realisation), with the blue dots representing the non-hysteretic case
421 and the red dots representing the hysteretic case. It can be seen from Figure 11 that
422 the results of the hysteretic case show larger variation. The variation is also not
423 limited along a single line in $\theta - h_s$ space, as in the non-hysteretic case, but varies in
424 a wider area. Note that, because k_{sat} was the only randomized parameter, the main
425 drying curve in the SWRC is the same for both the non-hysteretic and hysteretic cases.
426 This means that, in the non-hysteretic case, the spatial variability can only cause the
427 scattering of blue dots located along the main drying curve in the SWRC. However, in
428 the hysteretic case, the hysteretic behaviour allows the suction to vary along the
429 scanning curve. When the spatial variability is added into the hysteretic effect, this
430 causes the suction to vary in the area enclosed by the main drying and wetting
431 curves.

432 **5.3.2 Influence of hysteresis on the stability of the heterogeneous slope**

433 The factor of safety has been calculated for each realisation and a log-normal
434 distribution fitted to the resulting ensemble distribution of FOS. Table 4 gives the
435 mean μ_{FOS} and standard deviation σ_{FOS} of the FOS for both the non-hysteretic
436 and hysteretic cases. The mean of the FOS at all times was smaller for the hysteretic

437 case than for the non-hysteretic case. In addition, the standard deviation of the FOS
438 was usually higher for the hysteretic case. The reason is that, in the hysteretic case,
439 the hysteresis in the water retention behaviour induced much more variation in the
440 PWP and VWC, because the PWP and VWC could vary in the area enclosed by the
441 main drying and wetting curves. Therefore, the uncertainty in the FOS is larger for
442 the hysteretic case.

443 Figure 12 shows the cumulative distribution functions (CDF) of FOS for both the
444 non-hysteretic (dashed line) and hysteretic cases (solid line) at different times. The
445 limit value of the FOS (dash-dotted line) represents the FOS calculated in a
446 homogeneous non-hysteretic analysis based on the mean value of k_{sat} . From the
447 results in Figure 12, it is seen that if a deterministic method is used to analyse the
448 safety of the embankment slope, there is a high probability of overestimating the
449 FOS (in this case, by up to 20% compared to a 95% reliability). Moreover, based on
450 the comparison between the solid and dashed lines, it can be concluded that, if only
451 the heterogeneity is considered while the hysteretic effect in the SWRC is ignored,
452 the computed probability of slope failure would be lower. This proves that, although
453 the contribution to the variation in results due to the uncertainties in the material
454 properties and the hysteresis can be different (the former factor could be larger if
455 there are strong uncertainties in the parameters), both factors play an important role
456 and should be considered in the analysis.

457 **6 Conclusion**

458 The combined effect of hysteresis in the water retention behaviour and

459 heterogeneity of an unsaturated soil on the stability of an embankment under
460 transient seepage has been investigated. The stability and reliability of the
461 embankment shows significant differences with analyses which ignore either or both
462 of these factors.

463 Under the influence of both hysteresis and heterogeneity, the PWP and VWC in
464 the transient seepage process have a larger variation than would otherwise be the
465 case. Considering slope stability, in the initially drying condition, the mean of the FOS
466 for the hysteretic case is smaller than that of the non-hysteretic case. Moreover, the
467 standard deviation of the FOS is usually larger. It has been found that, due to
468 hysteresis in the water retention behaviour, the influence of the heterogeneity of soil
469 property values on slope stability could be amplified. Furthermore, in the sensitivity
470 analysis of hydraulic parameters, it was found the saturated hydraulic conductivity,
471 k_{sat} , plays a dominant role in slope stability compared to other hydraulic parameters.
472 Further studies on the impact of spatial variability on these processes are needed to
473 provide comprehensive conclusions.

474 **Acknowledgements**

475 The authors wish to acknowledge the support of the China Scholarship Council
476 coupled with the Geo-Engineering Section of Delft University of Technology for
477 financial support of the for the first author and a Marie Curie Career Integration
478 Grant, No. 333177, for the second author.

479

c'	effective cohesion
c'_f	factored effective cohesion at slope failure
COV	coefficient of variation
FOS	factor of safety
g	gravitational acceleration
G_s	specific gravity of the soil particles
h	pore water pressure head
h_s	suction head
$h_{s,ae}$	air-entry suction head
$h_{s,ae,d}$	air-entry suction head for the main drying curve
$h_{s,ae,w}$	air-entry suction head for the main wetting curve
k	hydraulic conductivity
k_{sat}	saturated hydraulic conductivity
k_x	hydraulic conductivity in the x direction
k_z	hydraulic conductivity in the z direction
l	scale of fluctuation
l_h	scale of fluctuation in the horizontal direction
l_v	scale of fluctuation in the vertical direction
m	fitting parameter for the soil water retention curve
MCM	Monte Carlo method
n	fitting parameter for the soil water retention curve

N	total number of realisations
N_f	number of realisations in which the slope fails
PWP	pore water pressure
s	matric suction
S	effective degree of saturation
SWRC	soil water retention curve
t	time
T_1	period of the first sinusoid
T_2	period of the second sinusoid
u_a	pore air pressure
u_w	pore water pressure
VGM	van Genuchten–Mualem model
VWC	volumetric water content
WL	water level
x	coordinate in the horizontal direction relative to upstream toe of embankment
z	coordinate in the vertical direction relative to upstream toe of embankment
α_d	approximately the inverse of the air-entry suction head for main drying curve
α_w	approximately the inverse of the air-entry suction head for main wetting curve
γ	unit weight of soil

γ_w	unit weight of water
θ	volumetric water content
θ_s	saturated volumetric water content
θ_r	residual volumetric water content
κ	slope of the scanning curve
μ	mean
ξ	degree of anisotropy of the heterogeneity
ρ	correlation coefficient between two points
ρ_w	density of water
σ	standard deviation
σ_t	total stress normal to the sliding plane
τ	shear stress
φ'	effective friction angle
φ'_f	factored effective friction angle at slope failure
χ	scalar defining the suction-induced effective stress

481 **References**

- 482 Arnold, P. and Hicks, M. A. (2010). Stochastic modelling of unsaturated slope stability. *Proceedings of*
 5th International Conference on Unsaturated Soils (UNSAT), Barcelona, 1237-1242.
- 483 Arnold, P. and Hicks, M. A. (2011). A stochastic approach to rainfall-induced slope failure. *Proceedings*
 of 3rd International Symposium on Geotechnical Safety and Risk, Munich, 107-115.
- 484 ASCE (2008). *Standard Guideline for Fitting Saturated Hydraulic Conductivity Using Probability Density*
 Functions, ASCE Standard ASCE/EWRI 50-08, ASCE, Reston.

-
- 488 Avanidou, T. and Paleologos, E. K. (2002). Infiltration in stratified, heterogeneous soils: Relative
489 importance of parameters and model variations. *Water Resources Research*, 38(11),
490 1232-1236.
- 491 Bishop, A. W. (1959). The principle of effective stress. *Teknisk Ukeblad*, 106(39), 859–863.
- 492 Cai, F. and Ugai, K. (2004). Numerical analysis of rainfall effects on slope stability. *International Journal*
493 *of Geomechanics*, 4(2), 69-78.
- 494 Carsel, R. F. and Parrish, R. S. (1988). Developing joint probability distributions of soil water retention
495 characteristics. *Water Resources Research*, 24(5), 755-769.
- 496 Celia, M. A., Bouloutas, E. T. and Zarba, R. L. (1990). A general mass-conservative numerical solution
497 for the unsaturated flow equation. *Water Resources Research*, 26(7), 1483-1496.
- 498 Chen, Q. and Zhang, L. M. (2006). Three-dimensional analysis of water infiltration into the Gouhou
499 rockfill dam using saturated unsaturated seepage theory. *Canadian Geotechnical Journal*,
500 43(5), 449-461.
- 501 Chen, Z., Govindaraju, R. S. and Kavvas, M. L. (1994a). Spatial averaging of unsaturated flow equations
502 under infiltration conditions over areally heterogeneous fields, 1, Development of models.
503 *Water Resources Research*, 30(2), 523– 533.
- 504 Chen, Z., Govindaraju, R. S. and Kavvas, M. L. (1994b). Spatial averaging of unsaturated flow equations
505 under infiltration conditions over areally heterogeneous fields, 2, Numerical simulations.
506 *Water Resources Research*, 30(2), 535– 548.
- 507 De Rooij, G. H., Kasteel, R. T., Papritz, A. and Flühler, H. (2004). Joint distributions of the unsaturated
508 soil hydraulic parameters and their effect on other variates. *Vadose Zone Journal*, 3(3),
509 947-955.

-
- 510 Ebel, B. A., Loague, K. and Borja, R. I. (2010). The impacts of hysteresis on variably saturated
511 hydrologic response and slope failure. *Environmental Earth Sciences*, 61(6), 1215-1225.
- 512 Fenton, G. A. and Vanmarcke, E. H. (1990). Simulation of random fields via local average subdivision.
513 *Journal of Engineering Mechanics*, 116(8), 1733-1749.
- 514 Freeze, R. A. (1975). A stochastic-conceptual analysis of one-dimensional groundwater flow in
515 nonuniform homogeneous media. *Water Resources Research*, 11(5), 725-741.
- 516 Gardner, R. H., O'Neill, R. V., Mankin, J. B. and Carney, J. H. (1981). A comparison of sensitivity analysis
517 and error analysis based on a stream ecosystem model. *Ecological Modelling*, 12(3), 173-190.
- 518 Griffiths, D. V. and Lane, P. A. (1999). Slope stability analysis by finite elements. *Géotechnique*, 49(3),
519 387-403.
- 520 Griffiths, D. V. and Fenton, G. A. (2004). Probabilistic slope stability analysis by finite elements. *Journal*
521 *of Geotechnical and Geoenvironmental Engineering*, 130(5), 507-518.
- 522 Gui, S., Zhang, R., Turner, J. P. and Xue, X. (2000). Probabilistic slope stability analysis with stochastic
523 soil hydraulic conductivity. *Journal of Geotechnical and Geoenvironmental Engineering*,
524 126(1), 1-9.
- 525 Han, X.-W., Shao, M.-A. and Horton, R. (2010). Estimating van Genuchten model parameters of
526 undisturbed soils using an integral method. *Pedosphere*, 20(1), 55-62.
- 527 Hicks, M. A. and Samy, K. (2002). Influence of heterogeneity on undrained clay slope stability.
528 *Quarterly Journal of Engineering Geology and Hydrogeology*, 35(1), 41-49.
- 529 Hicks, M. A. and Samy, K. (2004). Stochastic evaluation of heterogeneous slope stability. *Italian*
530 *Geotechnical Journal*, 38(2), 54-66.
- 531 Hicks, M. A. and Spencer, W. A. (2010). Influence of heterogeneity on the reliability and failure of a

-
- 532 long 3D slope. *Computers and Geotechnics*, 37(7), 948-955.
- 533 Jaynes, D. B. (1984). Comparison of soil–water hysteresis models. *Journal of Hydrology*, 75(1),
534 287-299.
- 535 Lam, L., Fredlund, D. G. and Barbour, S. L. (1987). Transient seepage model for saturated–unsaturated
536 soil systems: a geotechnical engineering approach. *Canadian Geotechnical Journal*, 24(4),
537 565-580.
- 538 Le, T. M. H., Gallipoli, D., Sanchez, M. and Wheeler, S. J. (2012). Stochastic analysis of unsaturated
539 seepage through randomly heterogeneous earth embankments. *International Journal for
540 Numerical and Analytical Methods in Geomechanics*, 36(8), 1056-1076.
- 541 Lehmann, F. and Ackerer, P. H. (1998). Comparison of iterative methods for improved solutions of the
542 fluid flow equation in partially saturated porous media. *Transport in Porous Media*, 31(3),
543 275-292.
- 544 Liu, K., Vardon, P. J., Arnold, P. and Hicks, M. A. (2015). Effect of hysteresis on the stability of an
545 embankment under transient seepage. *IOP Conference Series: Earth and Environmental
546 Science*, 26(1), 012013.
- 547 Ma, K. C., Tan, Y. C. and Chen, C. H. (2011). The influence of water retention curve hysteresis on the
548 stability of unsaturated soil slopes. *Hydrological Processes*, 25(23), 3563-3574.
- 549 Mualem, Y. (1976). A new model for predicting the hydraulic conductivity of unsaturated porous
550 media. *Water Resources Research*, 12(3), 513-522.
- 551 Nakagawa, K., Saito, M. and Berndtsson, R. (2012). On the importance of hysteresis and heterogeneity
552 in the numerical simulation of unsaturated flow. *Hydrological Research Letters*, 6, 59-64.
- 553 Nielsen, D. R., Biggar, J. W. and Erh, K. T. (1973). Spatial variability of field-measured soil–water

-
- 554 properties. *Hilgardia*, 42, 215-259.
- 555 Pham, H. Q., Fredlund, D. G. and Barbour, S. L. (2005). A study of hysteresis models for soil–water
556 characteristic curves. *Canadian Geotechnical Journal*, 42(6), 1548-1568.
- 557 Phoon, K.-K. and Kulhawy, F. H. (1999). Characterization of geotechnical variability. *Canadian
558 Geotechnical Journal*, 36(4), 612-624.
- 559 Phoon, K.-K., Santoso, A. and Quek, S.-T. (2010). Probabilistic analysis of soil–water characteristic
560 curves. *Journal of Geotechnical and Geoenvironmental Engineering*, 136(3), 445-455.
- 561 Rahardjo, H., Ong, T., Rezaur, R., and Leong, E. C. (2007). Factors controlling instability of
562 homogeneous soil slopes under rainfall. *Journal of Geotechnical and Geoenvironmental
563 Engineering*, 133(12), 1532-1543.
- 564 Rahardjo, H., Nio, A. S., Leong, E. C. and Song, N. Y. (2010). Effects of groundwater table position and
565 soil properties on stability of slope during rainfall. *Journal of Geotechnical and
566 Geoenvironmental Engineering*, 136(11), 1555-1564.
- 567 Russo, D. and Bouton, M. (1992). Statistical analysis of spatial variability in unsaturated flow
568 parameters. *Water Resources Research*, 28(7), 1911-1925.
- 569 Santoso, A. M., Phoon, K.-K. and Quek, S.-T. (2011). Effects of soil spatial variability on rainfall-induced
570 landslides. *Computers and Structures*, 89(11), 893-900.
- 571 Sivakumar Babu, G. L. and Murthy, D. S. (2005). Reliability analysis of unsaturated soil slopes. *Journal
572 of Geotechnical and Geoenvironmental Engineering*, 131(11), 1423-1428.
- 573 Smith, I. M., Griffiths, D. V. and Margetts, L. (2013). *Programming the finite element method*. John
574 Wiley and Sons, Chichester, UK, 5th edition.
- 575 Tami, D., Rahardjo, H. and Leong, E.-C. (2004). Effects of hysteresis on steady-state infiltration in

-
- 576 unsaturated slopes. *Journal of Geotechnical and Geoenvironmental Engineering*, 130(9),
- 577 956-967.
- 578 Tsai, T.-L. and Chen, H.-F. (2010). Effects of degree of saturation on shallow landslides triggered by
- 579 rainfall. *Environmental Earth Sciences*, 59(6), 1285-1295.
- 580 Tsaparas, I., Rahardjo, H., Toll, D. G. and Leong, E. C. (2002). Controlling parameters for rainfall-induced
- 581 landslides. *Computers and Geotechnics*, 29(1), 1-27.
- 582 Van Genuchten, M. T. (1980). A closed-form equation for predicting the hydraulic conductivity of
- 583 unsaturated soils. *Soil Science Society of America Journal*, 44(5), 892-898.
- 584 Vanapalli, S. K., Fredlund, D. G., Pufahl, D. E. and Clifton, A. W. (1996). Model for the prediction of
- 585 shear strength with respect to soil suction. *Canadian Geotechnical Journal*, 33(3), 379-392.
- 586 Wu, L. Z., Huang, R. Q. and Xu, Q. (2012). Incorporating hysteresis in one-dimensional seepage
- 587 modeling in unsaturated soils. *KSCE Journal of Civil Engineering*, 16(1), 69-77.
- 588 Yang, C., Sheng, D. and Carter, J. P. (2011). Hysteretic seepage analysis in unsaturated soil covers.
- 589 *Proceedings of 5th Asia-Pacific Conference on Unsaturated Soils*, Pattaya, 541-546.
- 590 Yang, C., Sheng, D. and Carter, J. P. (2012). Effect of hydraulic hysteresis on seepage analysis for
- 591 unsaturated soils. *Computers and Geotechnics*, 41, 36-56.
- 592 Yang, C., Sheng, D., Carter, J. P. and Huang, J. (2013). Stochastic evaluation of hydraulic hysteresis in
- 593 unsaturated soils. *Journal of Geotechnical and Geoenvironmental Engineering*, 139(7),
- 594 1211-1214.
- 595 Zhang, L. L. (2007). Effects of soil hydraulic hysteresis on slope reliability. *Proceedings of 1st*
- 596 *International Symposium on Geotechnical Safety and Risk (ISGSR 2007)*, Shanghai, 399-405.
- 597 Zhang, L. L., Fredlund, M. D., Fredlund, D. G., Lu, H. and Wilson, G. W. (2015). The influence of the

-
- 598 unsaturated soil zone on 2-D and 3-D slope stability analyses. *Engineering Geology*, 193,
- 599 374-383.
- 600 Zhang L., Li, J., Li, X., Zhang, J. and Zhu, H. (2016). *Rainfall-induced soil slope failure*. CRC Press, Boca
- 601 Raton.
- 602 Zhang, L., Zhang, L. and Tang, W. H. (2005). Rainfall-induced slope failure considering variability of soil
- 603 properties. *Géotechnique*, 55(2), 183-188.
- 604 Zhu, H., Zhang, L. M., Zhang, L. L. and Zhou, C. B. (2013). Two-dimensional probabilistic infiltration
- 605 analysis with a spatially varying permeability function. *Computers and Geotechnics*, 48,
- 606 249-259.

Table 1 Parameter values for the homogenous case.

Parameter	Symbol	Units	Value
Saturated hydraulic conductivity	k_{sat}	m/d	0.0864
VGM parameter for the main drying (and non-hysteretic) curve	α_d	m^{-1}	0.1
VGM parameter for the main wetting curve	α_w	m^{-1}	0.2
Fitting parameter for VGM model	n	-	1.226
Saturated VWC	θ_s	-	0.38
Residual VWC	θ_r	-	0.0038
Slope of the scanning curve	κ	m^{-1}	0.00006
Stiffness	E	kPa	1.0×10^5
Poisson's ratio	ν	-	0.3
Effective cohesion	c'	kPa	15
Effective friction angle	φ'	°	20
Specific gravity	G_s	-	2.02

Note: VGM represents the van Genuchten–Mualem model described in Section 2.2.

Table 2 Statistical distributions of the hydraulic parameters

Parameter	k_{sat} [m/d]	$ \alpha_d $ [m^{-1}]	n [-]	θ_s [-]	θ_r [-]
Distribution	Lognormal	Lognormal	Normal	Lognormal	Lognormal
μ	0.0864	0.1	1.226	0.38	0.0038
σ	0.0864	0.05	0.08	0.06	0.0002
COV	1.0	0.5	0.065	0.16	0.053

Table 3 Outline of numerical investigation

Sub-section	Hysteresis	Parameter sensitivity	Spatial variability
5.1	✓		
5.2	✓	✓	
5.3	✓		✓

Table 4 Statistical information of the FOS based on 1000 realisations

Case	Time t	μ_{FOS}	σ_{FOS}	Case	Time t	μ_{FOS}	σ_{FOS}
Hysteretic	$1T_2$	1.199	0.0374	Non-hysteretic	$1T_2$	1.221	0.0364
	$2T_2$	1.233	0.046		$2T_2$	1.278	0.045
	$T_1 = 3T_2$	1.182	0.0467		$T_1 = 3T_2$	1.245	0.0488
	$4T_2$	1.232	0.049		$4T_2$	1.274	0.0475
	$5T_2$	1.253	0.0535		$5T_2$	1.311	0.0529

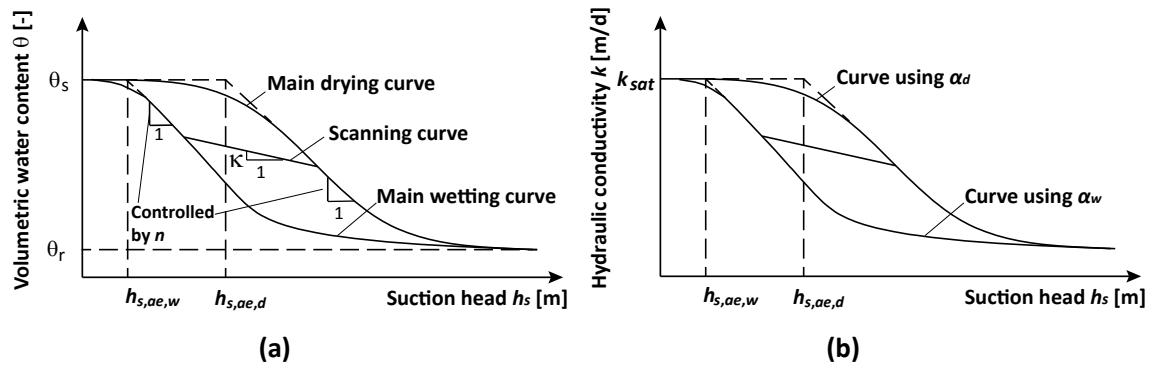


Figure 1. The relationships between suction head and: (a) VWC, and (b) hydraulic conductivity.

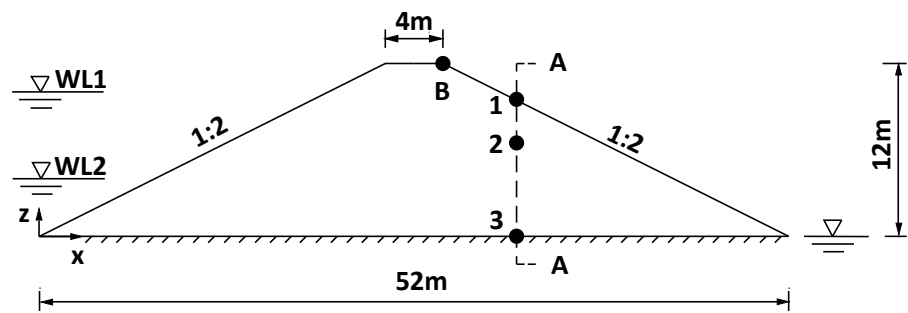


Figure 2. Geometry of the embankment.

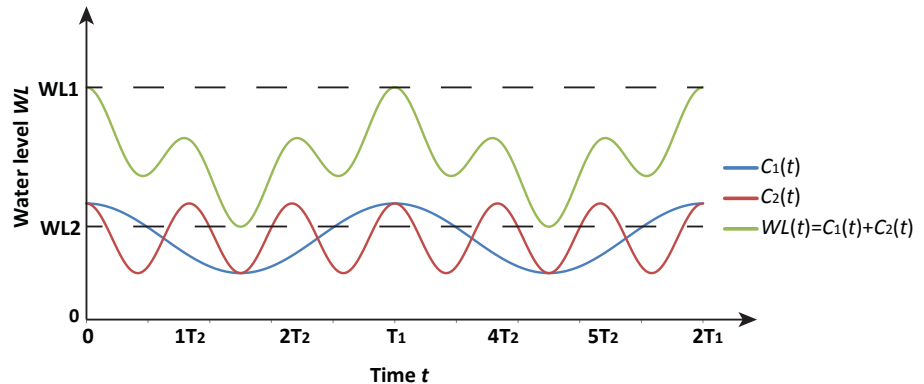


Figure 3. Water level fluctuation simulated by the sum of two sinusoidal curves.

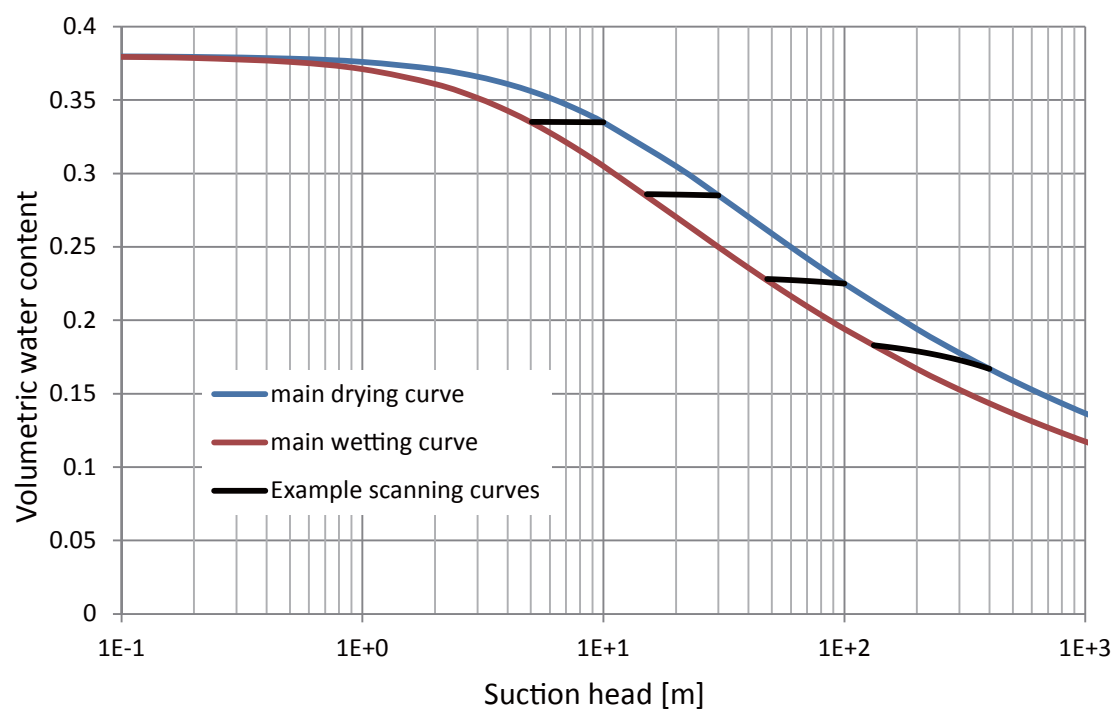


Figure 4. SWRC used in the analyses

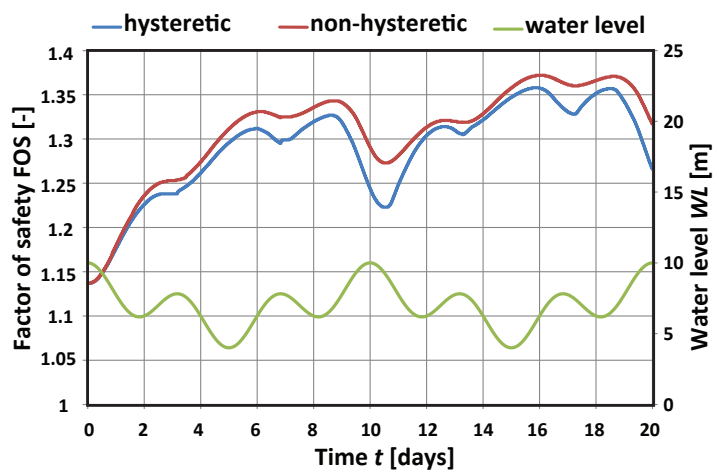


Figure 5. FOS variation with time.

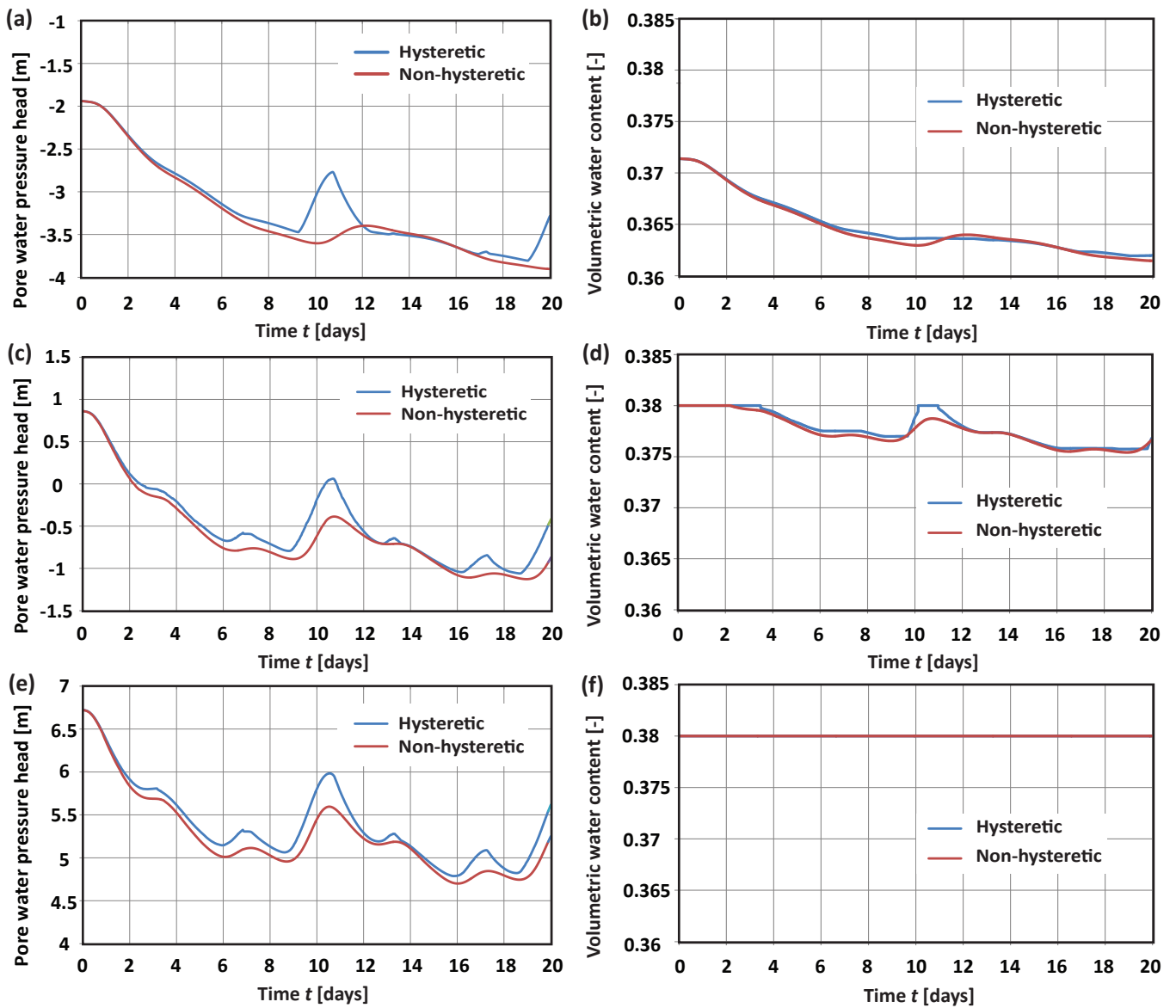


Figure 6. PWP head and VWC versus time at different depths (points 1-3 in Figure 2): (a) and (b) $z_1 = 9\text{ m}$; (c) and (d) $z_2 = 6\text{ m}$; and (e) and (f) $z_3 = 0\text{ m}$.

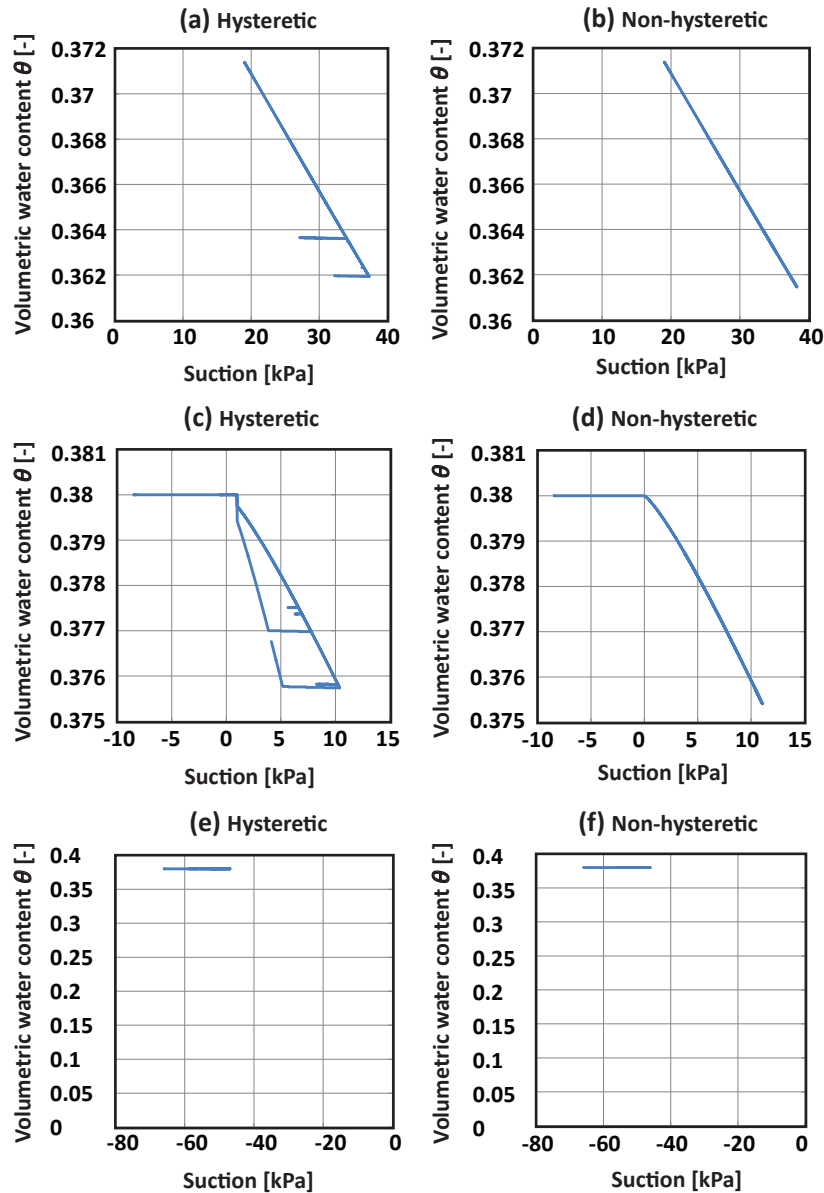


Figure 7. VWC versus suction at points along profile A-A at different depths: (a) and (b) $z_1 = 9\text{ m}$; (c) and (d) $z_2 = 6\text{ m}$; and (e) and (f) $z_3 = 0\text{ m}$.

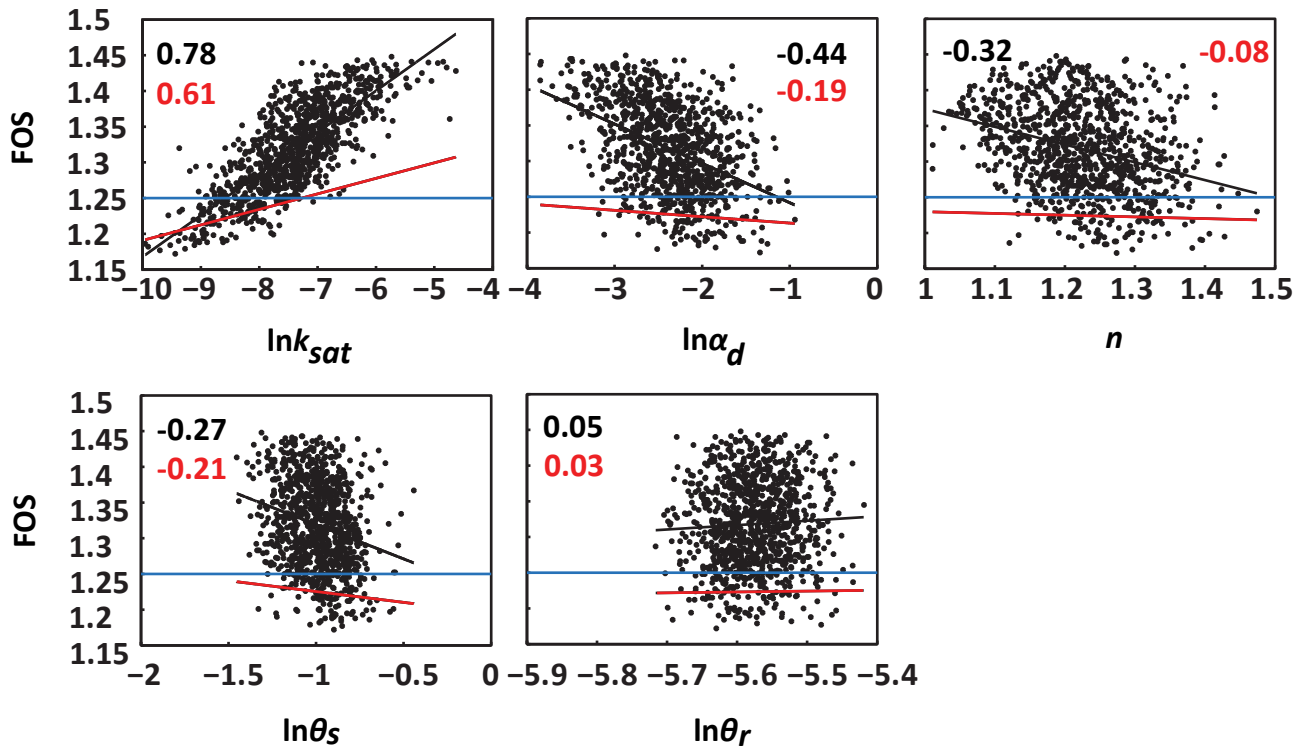


Figure 8. Correlation between FOS and different hydraulic parameters for non-hysteretic case at $t = 2T_2$. (The blue line represents $FOS = 1.25$, the black line and black number represent the correlation based on all the FOS values, and the red line and red number represent the correlation based on FOS values lower than $FOS = 1.25$).

Parameter	Curves	Relation
θ_s	1, 2	$\theta_{s1} > \theta_{s2}$
α_d	2, 4	$\alpha_{d2} < \alpha_{d4}$
n	2, 3	$n_2 < n_3$

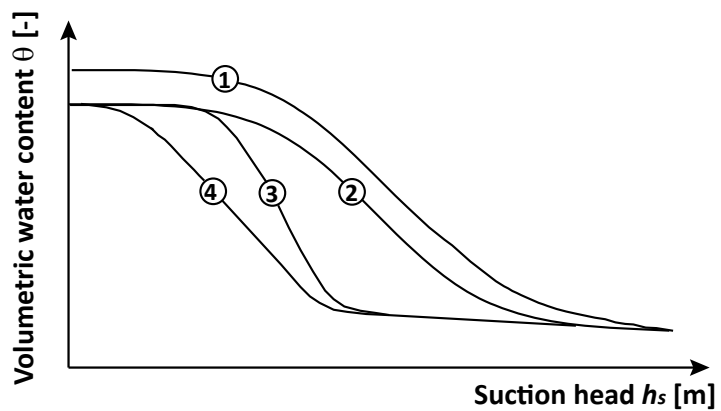


Figure 9. Sensitivity of the SWRC equation to model parameters.

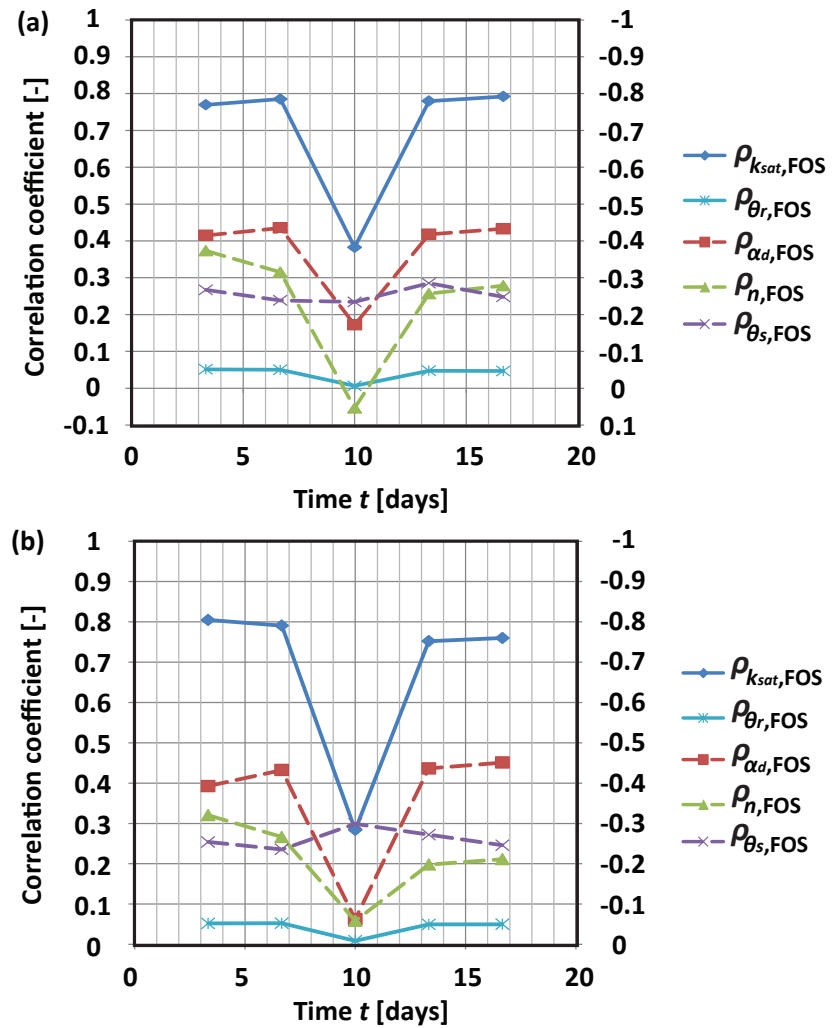


Figure 10. Correlation coefficients between FOS and different hydraulic parameters at several specific times: (a) non-hysteretic case and (b) hysteretic case.

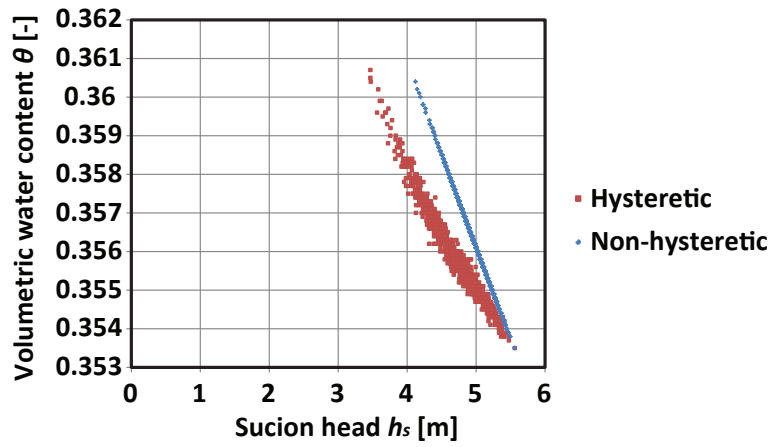


Figure 11. VWC versus suction head at Point B at $t = T_1 = 10$ d based on 1000 realisations.

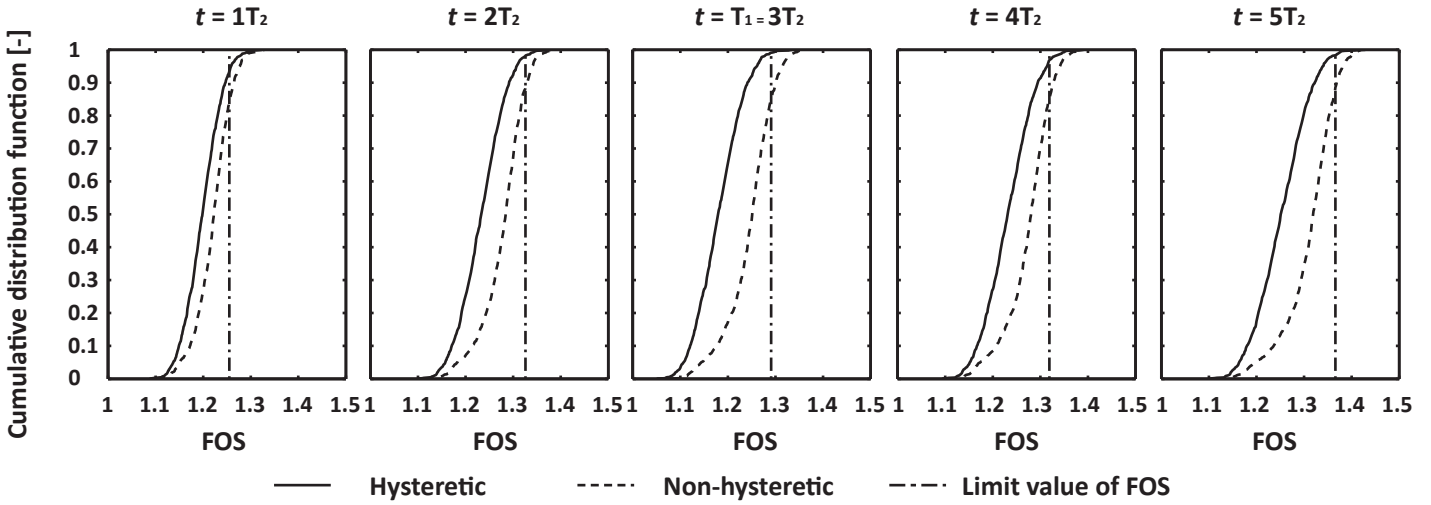


Figure 12. Cumulative distribution functions (CDFs) of FOS for both non-hysteretic and hysteretic cases at different times. The solid line is the CDF for the hysteretic case and the dotted line is for the non-hysteretic case. The dash-dotted line shows the factor of safety calculated without considering heterogeneity or hysteresis.